Phys. Med. Biol. **42** (1997) 2577–2589. Printed in the UK PII: S0031-9155(97)83083-7

Automated detection of clustered microcalcifications on mammograms: CAD system application to MIAS database

Norhayati Ibrahim†, Hiroshi Fujita†, Takeshi Hara† and Tokiko Endo‡

† Department of Information Science, Faculty of Engineering, Gifu University, Yanagido, Gifu 501-11, Japan

‡ Department of Radiology, Nagoya National Hospital, Naka-ku, Nagoya 460, Japan

Received 26 March 1997, in final form 20 August 1997

Abstract. To investigate the detection performance of our automated detection scheme for clustered microcalcifications on mammograms, we applied our computer-aided diagnosis (CAD) system to the database of the Mammographic Image Analysis Society (MIAS) in the UK. Forty-three mammograms from this database were used in this study. In our scheme, the breast regions were firstly extracted by determining the skinline. Histograms of the original images were used to extract the high-density area within the breast region as the segmentation from the fatty area around the skinline. Then the contrast correction technique was employed. Gradient vectors of the image density were calculated on the contrast corrected images. To extract the specific features of the pattern of the microcalcifications, triple-ring filter analysis was employed. A variable-ring filter was used for more accurate detection after the triple-ring filter. The features of the detected candidate areas were then characterized by feature analysis. The areas which satisfied the characteristics and specific terms were classified and displayed as clusters. As a result, the sensitivity was 95.8% with the false-positive rate at 1.8 clusters per image. This demonstrates that the automated detection of clustered microcalcifications in our CAD system is reliable as an aid to radiologists.

1. Introduction

Breast cancer is fast becoming the most dangerous women's cancer in Japan due to the westernization of life style. Palpation was formerly the only practical detection method but usually only managed to detect the lesion at an advanced stage. Mammography is at present the most effective method for early detection of breast cancer. A reduction in breast cancer deaths of about 30% can be achieved by screening (Daniel 1989). Mammography is able to visualize non-palpable and often minimal tumours smaller than 0.5 cm (Dhawan *et al* 1996). However, retrospective studies have shown that radiologists do not detect all breast cancers that are visible on the mammograms (Chan *et al* 1995). It is believed that microcalcifications could indicate an early stage of breast cancer; they are basically markers for early detection of some breast cancers in asymptomatic women (Dhawan *et al* 1996).

Many studies have been made to aid radiologists' interpretation of mammograms, especially at the stage of microcalcifications. Double reading of mammograms is very helpful and may improve radiologists' performance. A computerized image analysis system might also be useful for improving the interpretation. In mammographic image analysis, computerized systems are currently employed for the detection of masses and clustered microcalcifications, and classification of mammographic lesions.

0031-9155/97/122577+13$19.50

A number of research groups have been investigating an automated method for improving radiologists' diagnosis of mammograms by developing computerized systems. Giger (1993) and Vyborny *et al* (1994) reviewed the utilization of computer vision and artificial intelligence for the development of computer-aided diagnosis (CAD) in mammography. We also believe that CAD must come to be important as a second line of attack in the diagnosis of mammograms given the rapid pace of development of computer technology at present. We have therefore been developing an effective automated detection scheme for masses and clustered microcalcifications in the mammograms of Japanese women, and also for classification of the lesions. In our CAD system all the images were digitized at a pixel size of 0.1 mm with 10-bit density resolution. We also analysed the computed radiography (CR) images which are officially usable as the mammography database of the Japan Society of Computer Aided Diagnosis of Medical Images (CADM), and obtained magnificent results. Our method for the detection of clustered microcalcifications is based on density gradients and a triple-ring filter (Hirako *et al* 1994, 1995a). Microcalcification is detected from a two-dimensional density-gradient image by analysing vector patterns that are similar to the shape of the microcalcification.

Many methods have been proposed for mammogram CAD systems (Giger 1993, Vyborny *et al* 1994). All investigators always espouse their own new methods, and it is not easy to evaluate their performance as a CAD system. This is mainly because each group usually employs their own database; some consist of a small number of mammograms and some include cases with only easily detectable lesions. One way to solve this issue is to use a common database and to discuss their results using this database.

In the present study, to evaluate the 'detectability potential' of the system we applied our scheme to the database of the Mammographic Image Analysis Society in the UK (called the MIAS database) (Suckling *et al* 1994). This dataset was employed to analyse the performance of our system in the detection of only the clustered microcalcifications.

In section 2 the MIAS database is briefly described. Methods used are summarized in section 3. Details can be found in previous papers (Hara *et al* 1996, Hirako *et al* 1994, 1995a, b, 1996a, b, Fujita *et al* 1995), though most of them were written in Japanese. Section 4 explains the results obtained from this application and includes discussion, and the last section is the conclusion of this study.

2. MIAS database†

Each of the mammograms in the MIAS database was obtained from the medio-lateral oblique view and was digitized to a spatial resolution of 0.05 mm pixel size with 8-bit density resolution. Four image sizes were provided, depending on the breast sizes: small (4320 pixel × 1600 pixel), medium (4320 pixel × 2048 pixel), large (4320 pixel × 2600 pixel) and extra large (5200 pixel × 4000 pixel).

Digitization was performed on a Joyce-Loeble scanning microdensitometre (SCANDIG-3) which has a linear response in the range 0.0 to 3.2 optical densities. The mammograms had been carefully selected from the United Kingdom National Breast Screening Programme. Unfortunately, from the 322 digitized images (161 patients) of the MIAS database, only 249 images were included in our tape. To investigate the performance of our CAD system in the detection of clustered microcalcifications, 43 images (19 abnormal images with only microcalcifications and 24 normal images) were used from the obtained 249 digitized images. These 43 images had been classified depending on the character of

† Details in Web Browse homepage: http://s20c.smb.man.ac.uk/services/MIAScom.html

background tissues into three categories, fatty ($n = 12$), fatty-glandular ($n = 12$), and dense ($n = 19$) in the database, and included a mixture of benign ($n = 8$) and malignant ($n = 11$) cases where three cases contained two clusters and one case contained three clusters which made a total of 19 images containing 24 clusters. From the list given there were in fact 25 images containing 30 locations of microcalcifications that could be verified as abnormal images, but three of the database were not included in the tape, two were not used because there was no specific location given, and one more image was defined by us as normal because there was no cluster but only two big benign calcifications. Twenty-four images were defined by us as normal cases, including the image which contained no cluster but two benign calcifications. In this study the other side (left or right) of the microcalcification images were employed as normal images. Please refer to the appendix for a comparison of the data used for the present study with the dataset given.

3. Methods

To be able to apply our schemes to the MIAS database, each of the mammograms was first compressed to an image with a pixel size of 0.1 mm. So that, for example, the 4320 pixel × 1600 pixel mammograms became 2160 pixel × 800 pixel images. Each of them was then linearly converted to pixel values of 1024 (ten bits), and for further procedures these mammograms were employed as original images. Figure 1 shows the flowchart of our overall scheme for detecting clustered microcalcifications.

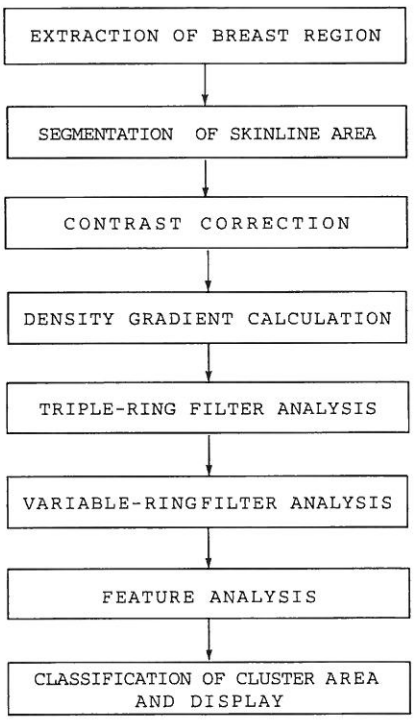

Figure 1. Flowchart of the overall scheme for detecting clustered microcalcifications.

3.1. Extraction of breast region

To reduce the data of digital images and to limit the required area for the detection, the border of the skinline in each mammogram was extracted by investigating the change of density profile (Kato *et al* 1997). The smallest rectangle containing the breast region was automatically extracted for further processing.

3.2. Segmentation of skinline area

For the segmentation of the skinline area from the breast area to limit the area for analysis, we divided the breast region into two areas—skinline area without microcalcifications and fatty and mammary gland areas. By using a density value histogram of the whole breast region, within the already extracted image, we decided upon the pixel value about 70% from the lowest pixel value as a threshold for determining the low-density area. The remaining 30% of the higher pixel value was extracted as the high-density area. Only the low-density area containing the suspicious microcalcifications was analysed.

3.3. Contrast correction

In this study, the contrast was defined as the difference between the minimum pixel value of a microcalcification and its background pixel value. In our previous papers (Hirako *et al* 1995a, 1996b), we found that there was a wide variation in the contrast of microcalcifications depending on the surroundings, such as tissue types and background density value. We believed that this situation occurred because of the contrast characteristic of the film used and the location of microcalcifications. If microcalcifications exist in a denser mammary gland area, higher absorption and dispersion of the x-ray beam in the surrounding tissues affect the contrast of the microcalcifications. This means that the contrast of the microcalcifications becomes less than it should be (Hirako *et al* 1996b). So, we analysed the contrast of each microcalcification and the background pixel value. Here we used 20 mammograms that included about 423 'true' microcalcifications and plotted the contrast values of each pixel. Figure 2 shows these data and the approximated one-dimensional curve for the analysis. The approximation obtained is

$$y = ax + b. \tag{1}$$

From this function we calculated the ratio r of the curve to the basic contrast s to correct the contrast of all microcalcifications. The ratio is given by

$$r = s/(ax + b). \tag{2}$$

We then used a contrast correction technique by using the approximated contrast correction curve

$$y = s(1 - a/2)\log(ax + b) + c \tag{3}$$

where $s = 45.0$, $a = 0.18719$, $b = 10.217$ and c is a constant which was obtained from the integral calculation of equation (2). This is a procedure where each pixel's contrast is corrected to the selected basic contrast s by the ratio r. The result is shown in figure 3. It should be noted that the slope of the curve in figure 3, the differential of the curve, coincides with the value of r. All of the original mammograms used were then corrected by this approximation.

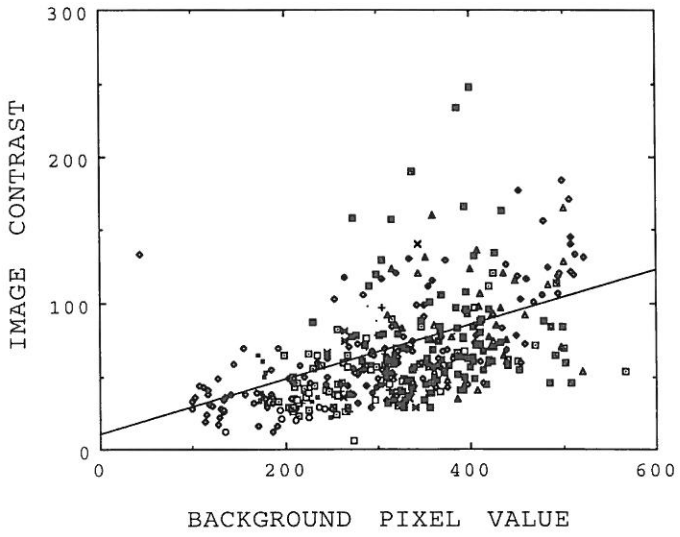

Figure 2. Dispersion of image contrast of each microcalcification depending on the background pixel value. The one-dimensional approximation of image contrast in terms of pixel value, obtained from 20 images, consisted of about 423 'true' microcalcifications, is shown. Different symbols show different image data.

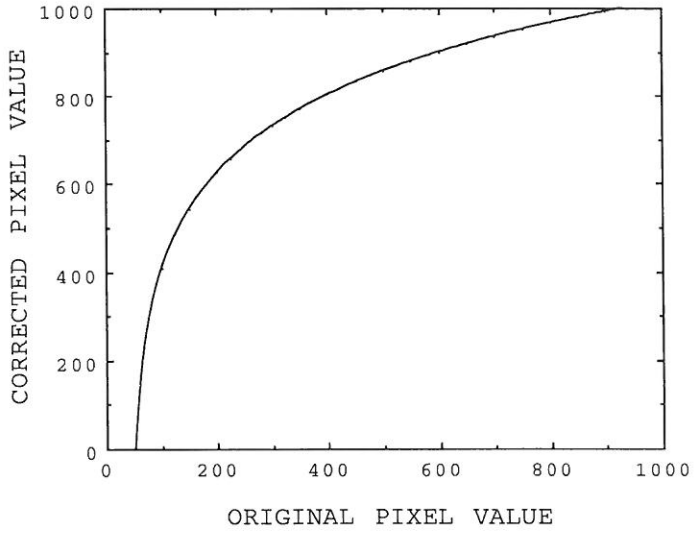

Figure 3. Contrast correction curve obtained by integral calculation of ratio r for the curve shown in figure 2.

3.4. Density gradient calculation

Microcalcifications are very small, less than 0.75 mm in diameter. In digitized images, even when dealing with 'blurred' images, microcalcifications are always smaller than

10 pixels in diameter, extremely small signals to be detected. The signal intensity of the microcalcification is also small in terms of density (pixel value) compared with that of its surrounding tissues. Basically, its density gradient is concentrated in the central area and constructs a particular cone-shaped vector pattern as shown in figure 4. This basic pattern was used as the typical shape of a microcalcification because both direction and magnitude components of the gradient vector are good features representing the presence of microcalcifications (Hirako *et al* 1995a). To calculate the components of the gradient vector, a Sobel filter was used on contrast corrected images. The Sobel filter is a type of edge-detection filter and has the advantage of providing both a differencing and a smoothing effect (Gonzalez and Woods 1992).

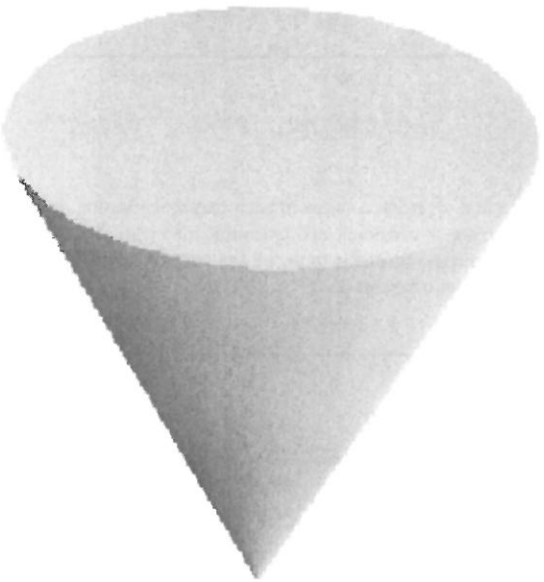

Figure 4. Typical density shape of a microcalcification. The circular cone structure is the property inherent in microcalcification shadows. It is anticipated that the microcalcification pattern can be detected if the region with a structure close to the circular cone is effectively extracted based on the gradient vector of the density fall in the breast area (Hirako *et al* 1995a).

3.5. Analysis of gradient vectors by a triple-ring filter

A triple-ring filter was used to analyse the calculated density gradient. This filter is composed of three different sizes of ring-shape subfilters which are three pixels (filter A), five pixels (filter B) and seven pixels (filter C) in diameter, as shown in figure 5. These subfilters are designed corresponding to various sizes of microcalcification. To analyse the density gradient, this triple-ring filter was superimposed iteratively on every pixel in the gradient-vector image. Calculated vector patterns, direction and magnitude values in each subfilter were then compared with the basic vector pattern. In this procedure, two features called the 'directional feature' and the 'magnitude feature' were determined as follows.

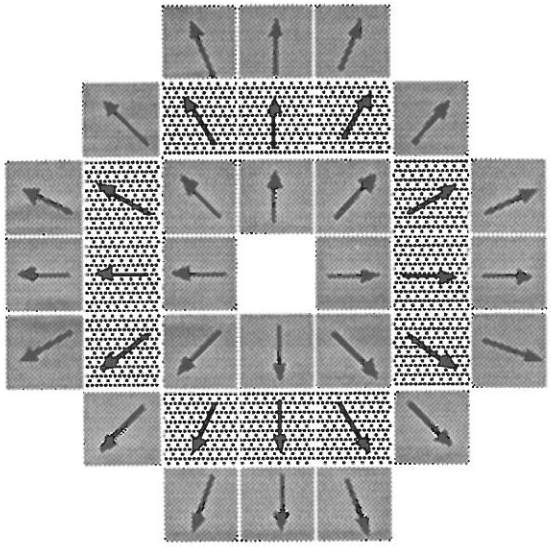

Figure 5. A triple-ring filter shown with the basic vector pattern for a typical microcalcification.

3.5.1. Calculation of the directional feature. The directional feature was calculated as follows. Firstly, the pixels were numbered according to the number of pixels in a subfilter. Let a vector at a pixel with the kth address on the subfilter written as V_k and the difference of its direction from basic vector pattern be $\theta_k (0 \leqslant \theta_k \leqslant \pi)$. Seventeen directions were determined for this procedure. Then a directional feature D was determined from the average of a directional feature component $d[= (1 + \alpha \sin\theta_k)\cos\theta_k]$. So the directional feature D for a subfilter composed of n pixels is given by

$$D = \frac{1}{n}\sum_{k=1}^{n}(1 + \alpha \sin\theta_k)\cos\theta_k \tag{4}$$

where $n = 8$ for filter A, $n = 12$ for filter B and $n = 16$ for filter C. D takes a value from -1 to 1. It approaches 1 when a candidate pattern is closer to the basic pattern and -1 when it is not. By setting the directional feature coefficient α to have a different value for each subfilter, the weight for the directional feature was adjusted depending on the subfilter, so even the vector patterns of the irregularly shaped microcalcifications were able to be observed (Hirako *et al* 1995a).

3.5.2. Calculation of the magnitude feature. Generally microcalcifications absorb more x-rays than the glandular tissues or blood vessels. In other words, the degree of decrease of the density gradient, the magnitude value, becomes greater in microcalcifications. The magnitude of a gradient vector is less affected by the size of microcalcifications but shows a ring-like shape. This density feature was utilized as the magnitude feature. In the calculation of the magnitude feature I, the direction feature was also considered. It can be obtained for each subfilter by the average of the directional feature components produced by each pixel of the subfilters and the magnitude of the vector V_k as shown below

$$I = \frac{1}{n}\sum_{k=1}^{n}|V_k|(1 + \alpha \sin\theta_k)\cos\theta_k. \tag{5}$$

3.5.3. Detection of possible microcalcifications. After the directional and magnitude features in each subfilter were calculated, those features were recalculated by the combination of the three subfilters, and the threshold values for detecting candidates microcalcifications were employed for these values. Three types of the subfilter combinations were used as given below:

directional feature of (filter A + filter B)/2 = a
directional feature of (filter B + filter C)/2 = b
directional feature of (filter A + filter B + filter C)/3 = c
magnitude feature of (filter A + filter B)/2 = d
magnitude feature of (filter B + filter C)/2 = e
magnitude feature of (filter A + filter B + filter C)/3 = f.

In this experiment, the threshold values for a, b and c were set as 0.81, 0.81 and 0.79 respectively. Threshold values for d, e and f were equal at 30. These threshold values were determined corresponding to a vector feature which became larger when the deepest part of the microcalcification was being analysed by the triple-ring filter.

3.6. Variable-ring filter analysis

A variable-ring filter was then superimposed on the candidate microcalcifications which were detected by the triple-ring filter. Since the weight α was adjusted during use of triple-ring filter in order to detect the irregularly shaped microcalcifications, the filter was unable to differentiate the cross-linear patterns such as blood vessels or glandular tissue. This is because the vector pattern of these cross-linear patterns is very similar to the vector patterns of irregularly shaped microcalcifications.

A variable-ring filter was utilized for discriminating and reducing these false-positives. Basically, the variable-ring filter is ideal to use in the first stage of detection but it requires a long detection time. In fact it is hopeless when many possible subjects for detection are present. This is also one of the reasons why the variable-ring filter was utilized after the triple-ring filter analysis. The filter changes its shape while analysing each candidate detected by the triple-ring filter, based on a region growing technique in terms of the magnitude of density gradient. From a cross-sectional profile of a microcalcification, we are able to observe the distribution of the vector magnitude. The deepest part of a microcalcification has a minimum value of the magnitude feature, called a local minimum point, and the edge of the ring-shaped microcalcification has a maximum value, called a local maximum point. The variable-ring filter changed its shape according to this distribution of magnitude value when detecting the local maximum point. After the variable-ring filter changed its shape and the candidate microcalcification which satisfied certain criteria was extracted, this dynamic filter was also employed to recalculate the directional feature and the magnitude feature of the candidates without weighting. Thus, the variable-ring filter could accurately analyse each candidate's characteristics which happened to change according to their contrast features. So the filter was able to extract the irregularly shaped microcalcifications and discriminate the false-positives. By using the contrast corrected images, the average pixel value of each pixel within the filter was determined and this value was employed as a threshold value for image binarization.

3.7. Feature analysis

To reduce the number of false-positives which still existed even after variable-ring filter analysis, feature analysis was employed on those microcalcification candidates which were

already preserved as binary images. Using these images, two features, an area and the circularity of each candidate, were calculated. The contrast feature of the contrast corrected images was also calculated. The threshold value for the area of a microcalcification was determined as less than 50 pixels so as not to detect big benign calcifications. The circularity was represented by $4\pi \times (\text{area})/(\text{contour length})^2$. This value becomes larger when the shape of a candidate is close to a circle (maximum value is 1.0) and smaller when it is not a circle. The threshold value for this circularity was set as 0.5, so that the linear pattern tissues such as blood vessels and mammary ducts and their crossing-points can be eliminated. The threshold value for the contrast feature was set to the lowest value of 30 in terms of pixel value difference.

3.8. Classification of cluster area and display

The remaining microcalcifications were then judged on whether they appeared to be individual or clustered microcalcifications. A cluster area was automatically extracted when more than three microcalcifications existed in an area of 50 mm^2. This was based on the judgment of an expert radiologist. A cluster area was displayed by a cloud shape. Figure 6 shows two examples of detected clusters for the MIAS database.

Each of the detected clustered areas was then classified. The classification of a cancerous malignant cluster by our scheme was mainly based on the microcalcifications which are (i) very small in size, (ii) concentrated at a point, (iii) numerous, (iv) different in size, and (v) irregular in shape. The cancerous level of the clusters was shown by three different colours of the cloud shape, where red is for malignant cases, yellow for intermediate cases and blue for benign cases.

4. Results and discussion

We used 43 images from the MIAS database, which consisted of only microcalcifications, to evaluate the potential of our system as a regular step to analyse various kinds of database. Nineteen images were abnormal (which we considered to contain 24 clusters), and 24 images were classified as normal. From our experience and experiments we made for this database, we noticed that when the threshold value of the magnitude feature was fixed in the variable-ring filter, the detection performance was not greatly affected though we changed the threshold value of magnitude feature in the triple-ring filter. So, in the present study, we fixed the threshold value of the magnitude feature in the triple-ring filter at the lower limit in order to detect as many microcalcification candidates as possible. But it has to be noticed here that the threshold value of the magnitude feature in the triple-ring filter has to be fixed at a suitable value because the lower the value is, the more time it will take to detect the candidates. Then to investigate the detection performance of our scheme the threshold value of the magnitude feature in the variable-ring filter was varied.

Table 1 shows the results of the sensitivity of our system obtained by changing the threshold value of the 'magnitude feature' in the variable-ring filter. In this experiment the highest sensitivity of our system towards the MIAS database is 95.8% (23/24) at a false-positive rate of 1.84 (79/43) clusters per image. One cluster was unable to be detected by our scheme and we found that the microcalcifications were stuck to each other. However, we only managed to employ the MIAS database which had a small number of clustered microcalcifications. Although the sensitivity was higher than the sensitivity obtained from the other databases of Japanese women (94.3% at a false-positive rate of 0.64 cluster per

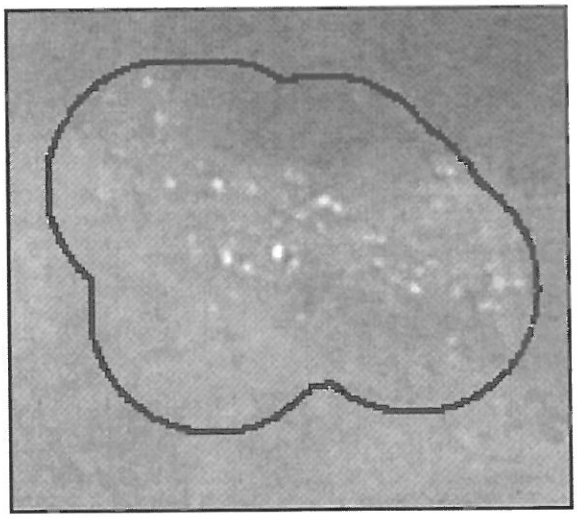

(a)

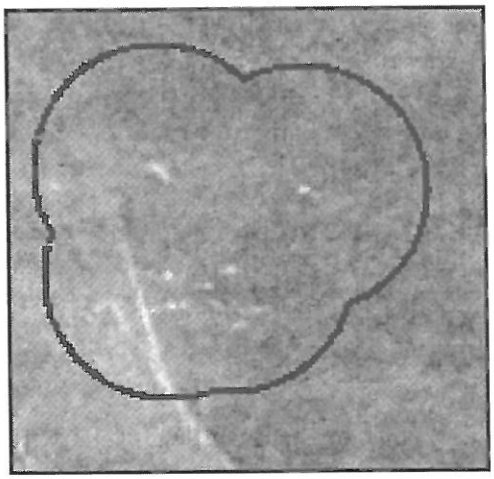

(b)

Figure 6. Two examples of detected clustered microcalcifications of (*a*) malignant and (*b*) benign cases, which were processed by contrast enhancement for easy visualization on the paper. The detected cluster area which contains more than three microcalcifications is shown by the cloud shaped full line. The white dots are the microcalcifications.

image), it is hard to decide whether our CAD system for breast cancer is effective for various databases. Using this scheme we were able to correctly classify about 70% (16/23) of the detected clustered areas, with 7 of the 16 clusters classified as intermediate cases by

Table 1. Results of true-positive (TP) and false-positive (FP) values obtained from MIAS database analysis when the threshold value for the 'magnitude feature' in the variable-ring filter is changed.

Magnitude feature	TP(%)	FP/image
60	66.6	0.14
50	87.5	0.70
49	87.5	0.93
46	91.6	1.63
41	91.6	1.72
39	95.6	1.84

the computer. We believe that our scheme could be improved to classify the MIAS database in the near future with a high correction rate.

The curve of contrast correction of the MIAS database is shown in figure 3. Here we used human sight aided by image processing to decide on the existence and locations of microcalcifications and the contrast feature. There is no detailed information on the exact location of each microcalcification and the number of microcalcifications given from the MIAS database. Only the centre coordinate and radius of a circle where the microcalcifications exist were provided. The contrast correction curve is also convenient when different cases or databases are used for testing because there are many parameters of the scheme which need to be readjusted for new cases. One way to facilitate this procedure was proposed mainly for the case in which the imaging characteristic in terms of contrast was different (Hirako *et al* 1996a). From the contrast correction curve shown in figure 3, we are able to see the difference between the MIAS database contrast and other institution's databases by comparing the pattern of the curves.

5. Conclusion

We applied our CAD system for mammograms to 43 digitized images of the MIAS database. We found that the sensitivity of our system is 95.8% with a false-positive rate at 1.84 clusters per image and that we have to reduce the false-positive rate and increase the database. Seventy per cent of the detected clustered microcalcifications were correctly classified. Further analysis has to be done for tuning certain threshold values for better classification analysis.

For the application of this system we only managed to employ one dataset (MIAS), but we are now working on other databases from different Japanese research groups and also a database from the United States. We are looking forward to utilizing many other databases in the future to evaluate our mammogram CAD system.

Acknowledgments

The authors are grateful to the Mammography Image Analysis Society in the UK for the database, Kenichi Hirako, MS, and Motohiro Kato, BS, for the programs, and all other members of Fujita Laboratory for their cooperation. This work was partly supported by the Grant-In-Aid for Cancer Research from the Ministry of Health and Welfare, the Telecommunications Advancement Foundation, and Suzuken Memorial Foundation.

Appendix

A.1. Employed database

The images that were employed for this study were mdb200rm to mdb249lm except for two images, mdb212rm and mdb214rs, for which no locations were verified. Images that were unable to be used for a certain reason (see section 2) for clustered microcalcifications were from mdb252rm to mdb256rl.

A.2. Division of images

The MIAS database is defined only by the location of the microcalcifications not clustered microcalcifications, and even the locations of microcalcification in one image were given by more than one coordinate; the abnormalities were verified as one case per image. In this study, all locations of microcalcifications given were defined as the number of clusters which exist to be detected. From the 19 images where mdb223ls, mdb239ll and mdb249lm contained two clusters, and mdb226rm contained three clusters, a total of 24 clustered areas were found. The sensitivity of this scheme was obtained by calculating the detected clustered areas divided by the 24 clustered areas from the 19 images.

References

Chan H P, Wei D, Helvie M A, Sahiner B, Adler D D, Goodsitt M M and Petrick N 1995 Computer-aided classification of mammographic masses and normal tissues: linear discriminant analysis in texture feature space *Phys. Med. Biol.* **40** 857–76

Daniel B K 1989 *Breast Imaging* (Philadelphia: Lippincott) vii–viii

Dhawan A P, Chitre Y, Kaiser-Bonasso C and Moskowitz 1996 Analysis of mammographic microcalcifications using gray-level image structure feature *IEEE Trans. Med. Imaging* **15** 246–59

Fujita H *et al* 1995 Automated-detection of masses and clustered microcalcifications on mammogram *Proc. SPIE* **2434** 682–92

Giger M L 1993 Computer-aided diagnosis *SYLLABUS: A Categorical Course in Physics: Technical Aspects of Breast Imaging* ed A G Haus and M J Yaffe (Oak Brook, IL: RSNA) pp 283–98

Gonzalez R C and Woods R E 1992 *Digital Image Processing* (Reading, MA: Addison-Wesley) pp 197–201, 418–20

Hara T, Hirako K, Fujita H, Endo T, Horita K, Ikeda M, Kido C and Ishigaki T 1996 Automated detection algorithm for clustered microcalcifications based on density gradient and triple-ring filter analysis *Digital Mammography '96* ed K Doi, M L Giger, R M Nishikawa and R A Schmidt (Amsterdam: Elsevier) pp 257–62

Hirako K, Fujita H, Endo T, Horita K, Kido C and Ishigaki T 1994 Development of detection filter based on density gradient analysis for mammographic microcalcifications *Med. Imaging Inform. Sci.* **11** 96–100 (in Japanese, with abstract and figure captions in English)

Hirako K, Fujita H, Hara T and Endo T 1995a Development of detection filter for mammographic microcalcifications: a method based on density gradient and triple-ring filter analysis *Trans. Inst. Electron. Inform. Commun. Eng. D-II* **J78-D-II** 1334–45 (in Japanese, with figure captions in English) (English transl 1996 *Syst. Comput. Japan* **17** (13) 36–48)

Hirako K, Fujita H, Endo T, Horita K, Kido C and Ishigaki T 1995b Extraction method of region of microcalcification candidate on mammograms by use of triple-ring filter analysis and region-growing technique *Med. Imaging Inform. Sci.* **12** 82–90 (in Japanese, with abstract and figure captions in English)

Hirako K, Fujita H, Hara T, Endo T and Horita K 1996a Automated detection of clustered microcalcifications on mammograms: strategy for image data from different facilities *Med. Imaging Inform. Sci.* **13** 54–60 (in Japanese, with abstract and figure captions in English)

Hirako K, Fujita H and Endo T 1996b Detection scheme for clustered microcalcifications with newly introduced contrast correction technique and variable-ring filter analysis *Med. Imaging Technol.* **14** 665–79 (in Japanese, with abstract and figure captions in English)

Kato M, Fujita H, Hara T and Endo T 1997 Improvement of automated breast-region extraction algorithm in a mammogram CAD system *Med. Imaging Inform. Sci.* **14** 104–13 (in Japanese, with abstract and figure captions in English)

Suckling J *et al* 1994 The mammographic image analysis society digital mammogram database *Digital Mammography* ed A G Gale, S M Astley, D R Dance and A Y Cairns (Amsterdam: Elsevier) pp 375–8

Vyborny C J and Giger M L 1994 Computer vision and artificial intelligence in mammography *Am. J. Roentgenol.* **162** 699–708